AGU PUBLICATIONS

Geophysical Research Letters

RESEARCH LETTER
10.1002/2016GL069605

Key Points:
- Three-dimensional structure of TC-induced upper ocean cooling is revealed with Argo data
- The magnitude and duration of TC-induced cooling depend on TC intensity, translation speed, and mixed layer depth
- The average cooling depth and total heat content induced by TCs are also calculated

Correspondence to:
G. Wang,
wghocean@yahoo.com

Citation:
Wang, G., L. Wu, N. C. Johnson, and Z. Ling (2016), Observed three-dimensional structure of ocean cooling induced by Pacific tropical cyclones, *Geophys. Res. Lett.*, *43*, 7632–7638, doi:10.1002/2016GL069605.

Received 16 MAY 2016
Accepted 7 JUL 2016
Accepted article online 12 JUL 2016
Published online 30 JUL 2016

Observed three-dimensional structure of ocean cooling induced by Pacific tropical cyclones

Guihua Wang[1,2], Lingwei Wu[2,3], Nathaniel C. Johnson[4], and Zheng Ling[2]

[1]Institute of Atmospheric Sciences, Department of Environmental Science and Enginnering, Fudan University, Shanghai, China, [2]State Key Laboratory of Satellite Ocean Environment Dynamics, Second Institute of Oceanography, State Oceanic Administration, Hangzhou, China, [3]Hangzhou College of Commerce, Zhejiang Gongshang University, Hangzhou, China, [4]Cooperative Institute for Climate Science, Princeton University, Princeton, New Jersey, USA

Abstract Sea surface cooling along tropical cyclone (TC) tracks has been well observed, but a complete understanding of the full three-dimensional structure of upper ocean TC-induced cooling is still needed. In this study, observed ocean temperature profiles derived from Argo floats and TC statistics from 1996 to 2012 are used to determine the three-dimensional structure of TC-induced cooling over the northwest Pacific. The average TC-induced sea surface temperature change derived from Argo reaches −1.4°C, which agrees well with satellite-derived estimates. The Argo profiles further reveal that this cooling can extend to a depth of ~30 m and can persist for about 20 days. The time scale of cooling recovery is somewhat longer in subsurface layers between a depth of ~10–15 m. Over the ocean domain where the mixed layer is shallower (deeper), the cooling is stronger (weaker), shallower (deeper), and more (less) persistent. The effect of initial MLD on the cooling derived from Argo observations may be only half of the idealized piecewise continuous model of tropical cyclone. These findings have implications for the total upper ocean heat content change induced by northwest Pacific TCs.

1. Introduction

The ocean response to tropical cyclones (TCs) has attracted much attention over the past several decades [*Fisher*, 1958; *Leipper*, 1967; *Brand*, 1971; *Price*, 1981; *Price et al*., 1994; *Dickey et al*., 1998; *Lin et al*., 2003; *Wada*, 2005; *Black and Dickey*, 2008; *Wada et al*., 2009; *Jansen et al*., 2010; *Dare and Mcbride*, 2011; *Vincent et al*., 2012]. One of the most striking phenomena of the ocean response to TCs is the dramatic sea surface cooling, with the coldest wake found on the rightside of the track. The cooling is due to intense vertical mixing (entrainment) and air-sea heat exchange. Both the intensity and translation speed of the TC are vital determinants of the extent of the sea surface cooling [*Brand*, 1971; *Price*, 1981; *Lin et al*., 2003; *Wada et al*., 2009]. Within days to weeks, the sea surface can recover to the temperature prior to the TC's passage through the subsequent atmospheric and oceanic processes [*Hazelworth*, 1968; *Nelson*, 1996; *Emanuel*, 2001; *Hart et al*., 2007; *Price et al*., 2008; *Dare and Mcbride*, 2011]. The turbulent mixing also often induces warming at the top of the thermocline, which persists longer than the surface cooling and results in a net heating of the ocean [*Price*, 1981; *Emanuel*, 2001; *Korty et al*., 2008; *Mei et al*., 2013].

The upper ocean cooling is important because it can suppress the development of TCs [*Bender et al*., 1993; *Wada and Chan*, 2008; *Lin et al*., 2013], including subsequent TCs that cross these cold wakes. The cooling typically ranges from 1 to 6°C [*Hazelworth*, 1968; *Price*, 1981; *Taira et al*., 1993; *Cione and Uhlhorn*, 2003; *Lin et al*., 2003; *Price et al*., 2008]. The sea surface cooling left behind the tropical cyclone can extend hundreds of kilometers adjacent to the storm track in the horizontal direction; vertically, the cooling depth is usually slightly thicker than the prestorm mixed-layer depth [*Large et al*., 1986].

Some satellites, especially those with microwave sensors, can observe the cooling at the surface, but measurements of the full three-dimensional structure of ocean temperature changes are more challenging. Some of the vertical structure has been documented through ship observations [*Hazelworth*, 1968], mooring arrays [*Dickey et al*., 1998], and aircrafts [*Price et al*., 1994]. With more and more hydrographic data available, it is time to study the complete three-dimensional structure of the cooling and to demonstrate how the cold wakes of tropical cyclones recover at different depths.

In this study, we document the observed three-dimensional structure of upper ocean cooling and recovery for northwest Pacific TCs as measured by an array of free-drifting Argo floats. Our motivation for focusing

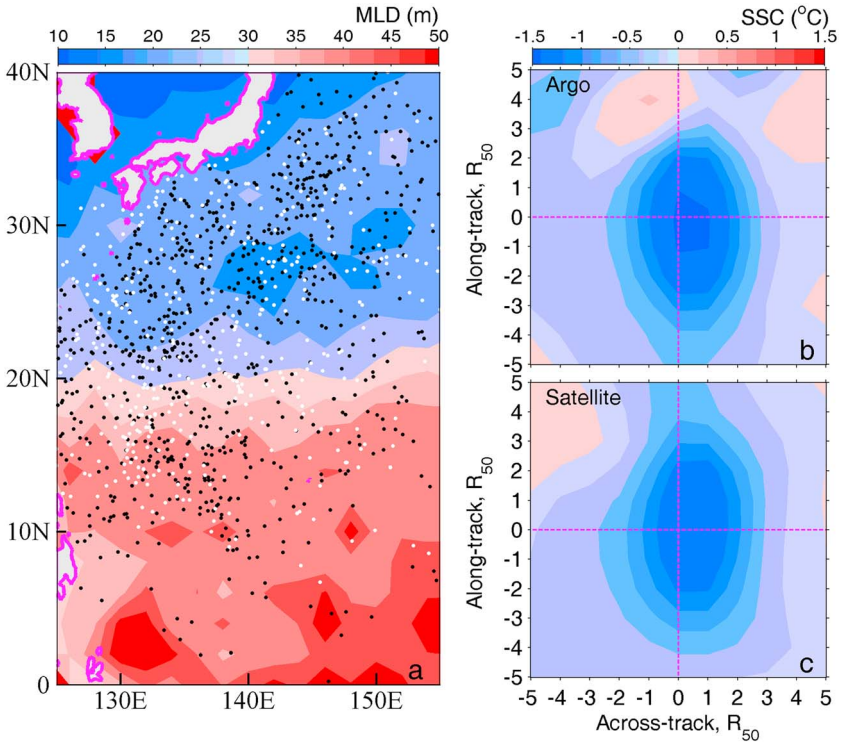

Figure 1. (a) Mixed layer depth (m, color shading) and distribution of Argo profiles (black dots) and TCs (white dots) from 1996 to 2013. (b) Sea surface cooling (°C) derived from Argo profiles. (c) As in Figure 1b but for satellite-derived measurements.

on the northwest Pacific is twofold: (1) this region is the most active basin for TCs, accounting for one third of all TCs between 1996 and 2012, and (2) this region is well observed through a dense network of Argo profiles (see Figure 1). Argo is a global array of drifting profiling floats that provide high-quality temperature and salinity profiles of the upper 2000 m of the ocean in near real time [*ARGO*, 2000]. In particular, the Argo system still can work under very hostile atmospheric and oceanic conditions such as TCs [*Roemmich and Owens*, 2000]. Thus, the Argo network provides an opportunity to describe the three-dimensional structure of the ocean cooling in response to TCs from an observational framework.

2. Data and Methods

Northwest Pacific TC statistics are derived from the best track data of the Japanese Meteorological Agency [http://www.jma.go.jp/jma/jma-eng/jma-center/rsmc-hp-pub-eg/trackarchives.html, also see *Barcikowska et al.*, 2012]. This data set includes the storm location, maximum sustained wind speed, and the longest radius of 50 knot (~26 m/s) wind (R_{50}). In order to normalize our results for the size of the TC, we only consider storms with 50 knot maximum sustained winds or stronger. We express TC size in units of R_{50}. In total, 258 of 391 tropical cyclones generated between 1996 and 2012 satisfy this criterion in the region of interest, which is defined as the box from 0°N to 40°N and from 120°E–180°E.

In the northwest Pacific region of this study, there are 111,773 Argo temperature profiles for the period 1996 to 2012. The data set used in this study is from the China Argo Real-time Data Center (http://www.argo.org.cn/), where the Argo data are sourced from the international Argo program (http://argo.jcommops.org). For all profiles, a real time and a delayed-mode quality control are conducted [*Tong et al.*, 2003]. We carried out an extra quality control to check for erroneous spikes, profile position, and suspicious profiles [*Wang et al.*, 2012].

To present the change of the ocean environment before and after TC passage, two paired profiles are identified through the following criteria: (1) only profiles with water depth greater than 1000 m are extracted to avoid coastal regions [*Park et al.*, 2011], (2) the distance between the TC and Argo profile must be within a

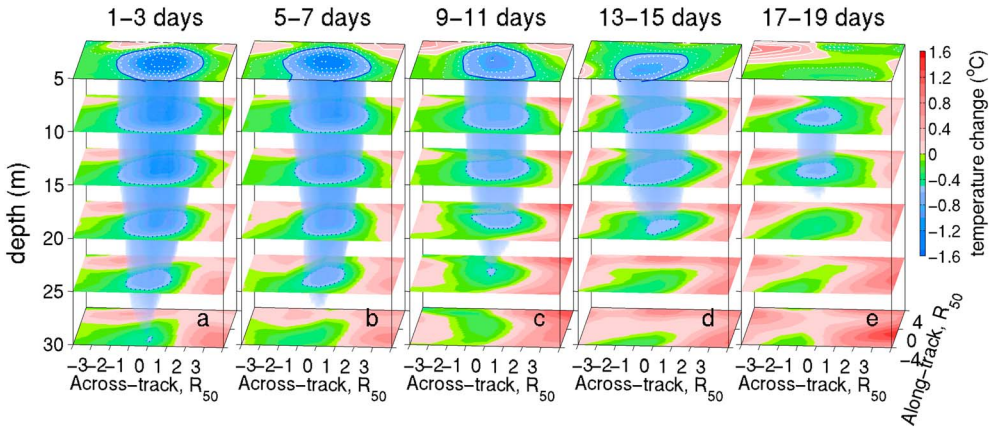

Figure 2. Time evolution of TC-induced three-dimensional cooling structure (°C): (a) 1–3 days, (b) 5–7 days, (c) 9–11 days, (d) 13–15 days, and (e) 17–19 days after TC passage. (R_{50} = 158 km).

search radius of $5R_{50}$, (3) the distance for the two paired profiles must be less than 200 km to minimize the anomalies due to background spatial ocean variability [*Park et al.*, 2011], and (4) for the temporal window, the pre-TC profile must be measured less than 10 days before TC passage [*Park et al.*, 2011] and the post-TC profile must be measured within several days (the time range is determined by the recovery time of the cooling, usually from 1 to 19 days) after TC passage. Following these sampling criteria, we identify a total of 1926 pairs of Argo profiles, sampling profiles from 258 different TCs. The relative locations between tropical cyclones and the paired profiles are estimated and are normalized to R_{50} of each tropical cyclone. The Cartesian coordinate is rotated into the storm-coordinate system, in which unit vectors are set to the along-track and cross-track directions. Because most of the sea surface cooling induced by TCs can make an *e*-folding recovery in 7 days and most of the local minimum SST occurs in 7 days [*Dare and Mcbride*, 2011], only the pairs (1029 pairs) between pre-TC profile and post-TC Argo profiles measured in 7 days after TC are used for our composites if not stated explicitly.

We also analyze satellite-derived sea surface temperature (SST) data from the National Oceanic and Atmospheric Administration (NOAA)/National Climate Data Center (details can be found in *Reynolds et al.* [2007]). This data set consists of daily observations on a 0.25° latitude-longitude grid.

To describe the cooling structure, we calculate the depth and area with the ocean cooling exceeding a threshold of −0.5°C. All parameters about the cooling structure such as cooling depth and area are based on the threshold. However, in calculating the accumulated surface heat content change, all layers from surface cooling downward to the layer where the cooling disappears (the temperature anomaly becomes positive) are extracted to integrate in each 5° × 5° grid.

3. Results

As mentioned in the introduction, an analysis of the northwest Pacific Ocean benefits from both frequent TC occurrence and high density of available Argo data. Both the Argo profiles and TCs are well distributed throughout the domain north of ~10°N (Figure 1a). Following the compositing procedure discussed in the previous section, we first compare the TC-induced surface cooling patterns derived from Argo profiles and satellite measurements. Figures 1b and 1c also illustrate the TC-induced surface cooling out to a radius of 5 R_{50} derived from Argo and satellite measurements (the mean R_{50} is 158 km with a standard deviation of 69 km). The patterns derived from both data sources are compared favorably, providing confidence that the Argo profiles are suitable for investigating TC-induced ocean temperature changes. The maximum sea surface cooling is −1.4°C for the composite, but this value ranges from −0.1°C to −5.5°C for individual TCs. The maximum cooling is located roughly 1.5 R_{50} from the TC center and in the right rear quadrant of the storm track, which is consistent with previous studies [*Price*, 1981; *Shay et al.*, 1992; *Black and Dickey*, 2008].

We next examine the full three-dimensional composite structure of TC-induced ocean cooling obtained from the Argo profiles. Figure 2a shows the composite change in ocean temperature extending to a depth of 30 m

Table 1. Maximum Surface Cooling, Area, and Interval of Cooling Exceeding −0.5°C Corresponding to Each Time Period Post-TC

Post-TC Period (days)	Maximum Surface Cooling (°C)	Area (km^2) of Surface Cooling	Cooling Interval (m)
1–3	−1.4	2.6×10^6	0–30
5–7	−1.3	7.7×10^5	0–27
9–11	−1	6.0×10^5	0–25
13–15	−0.9	4.7×10^5	0–20
17–19	> -0.5	0	10–15

and to a lag of 19 days after TC passage. Temperature changes less than −0.5°C are shaded in blue. The average cooling depth can extend to a depth of 30 m (Figure 2a). As the depth increases from 5 m to 30 m, the maximum cooling immediately following TC passage (Figure 2a) varies from −1.4°C to −0.5°C and the cooling area is also reduced from $2.6 \times 10^6 km^2$ to $1.2 \times 10^6 km^2$. The sea surface cooling is mainly due to entrainment, and the magnitude and extent of cooling vary with the strength, translation speed, and size of the TC [*Price*, 1981; *Oey et al*., 2006; *Black and Dickey*, 2008].

Following the rapid TC-induced cooling, SSTs gradually recover through atmospheric and oceanic processes, with the recovery time varying from days to weeks [*Hazelworth*, 1968; *Emanuel*, 2001; *Hart et al*., 2007]. Here we illustrate the full three-dimensional ocean temperature recovery for four post-TC lags: 5–7 days (Figure 2b), 9–11 days (Figure 2c), 13–15 days (Figure 2d), and 17–19 days (Figure 2e). The end of recovery period is defined when the composite ocean cooling exceeding −0.5°C disappears. In the days following TC passage, the surface cooling and cooling area are gradually reduced and the cooling depth becomes shallower. The values of maximum surface cooling, the area of surface cooling, and cooling interval are listed in Table 1. For the period of 17–19 days after TC passage, the temperature anomalies above 10 m and below 15 m nearly disappear, but they still persist in the layer between 10 m and 15 m. The surface cooling above 10 m disappears earlier because the ocean traps heat in the surface during recovery, while entrainment is important for the cooling recovery below 15 m. These observations suggest that the average recovery time of the cooling is around 20 days, which is quite similar to the previous studies [*Hazelworth*, 1968; *Nelson*, 1996; *Emanuel*, 2001; *Hart et al*., 2007], but this time scale is somewhat longer in subsurface layers between a depth of ~10–15 m.

As mentioned earlier, the magnitude and structure of the cooling for individual storms are expected to deviate from the composite structure depending on TC translation speed and intensity [*Price*, 1981; *Oey et al*., 2006; *Black and Dickey*, 2008]. Table 2 lists maximum surface cooling, the area of surface cooling, and cooling interval for slow/fast TCs and strong/weak TCs. As expected, slow ($U_h < 5.48$ m/s, which includes 311 samples moving more than 1 standard deviation slower from mean translation speed of all TCs) TCs can induce a larger, deeper, and stronger cooling than faster ($U_h > 10.11$ m/s, i.e., 197 samples moving more than 1 standard deviation faster than the mean translation speed) TCs (Figures 3a and 3b). Note that R_{50} in each panel is different in Figure 3. It is interesting to note that strong ($V_{max} > 81$ knots, 320 samples) TCs can induce a deeper cooling than weaker ($V_{max} < 66$ knots, 347 samples) TCs, but the cooling magnitude for strong TCs is slightly smaller for weak TCs (Figures 3c and 3d). The latter may be associated with the regions of TC occurrence. Most of strong (weak) TCs occur south (north) of 30°N, corresponding to the regions of deep (shallow) mixed layer depth (MLD). If TCs affect the region where the MLD is similar, strong TCs can induce a larger, deeper, and stronger cooling than weak TCs as expected (figure is omitted). Similar to the work done in *Price* [1981], we can estimate the maximum cooling by regressing it on the initial MLD. The regression coefficient is 0.03°C/m, which is only half of 0.06°C/m given by his idealized piecewise continuous model, suggesting that

Table 2. Maximum Surface Cooling, Area, and Interval of Cooling Exceeding −0.5°C Corresponding to Different TC Types

TC Types	Maximum Surface Cooling (°C)	Area (km^2) of Surface Cooling	Cooling Interval (m)
Strong TCs	−1.27	7.0×10^5	30
Weak TCs	−1.39	4.5×10^5	20
Fast TCs	−1.12	5.6×10^5	20
Slow TCs	−1.45	6.6×10^5	30
Deep MLD	−0.99	4.3×10^5	40
Shallow MLD	−1.65	1.1×10^6	20

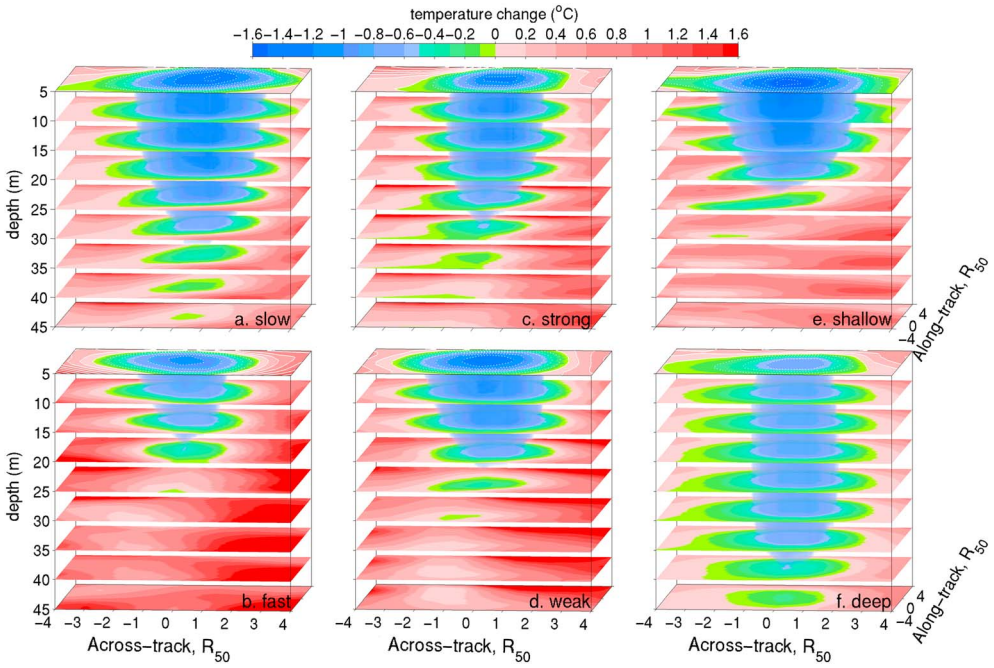

Figure 3. Ocean temperature change (°C) due to (a) slow, (b) fast, (c) strong, (d) weak tropical cyclones, and TC-induced ocean temperature change (°C) over the region where the mixed layer is (e) shallow and (f) deep. R_{50} are 186, 129, 161, 151, 149, and 160 km for Figures 3a–3f, respectively.

the effect of initial MLD on the cooling derived from observation may be smaller than the idealized model. This difference between observation and model needs to be explored further in the future.

Our analysis suggests that MLD also may exert a significant influence on TC-induced subsurface cooling. In particular, TCs can induce a larger entrainment rate and further produce a larger cooling in the region where the MLD is shallow [*Price*, 1981; *Ginis*, 2002]. To examine the impact of MLD on TC-induced ocean cooling, we perform similar composite analyses but for shallow (<30 m) and deep MLD (>30 m). Within this subset of 1029 profiles, 367 and 662 occurred in the deep and shallow MLD region, respectively.

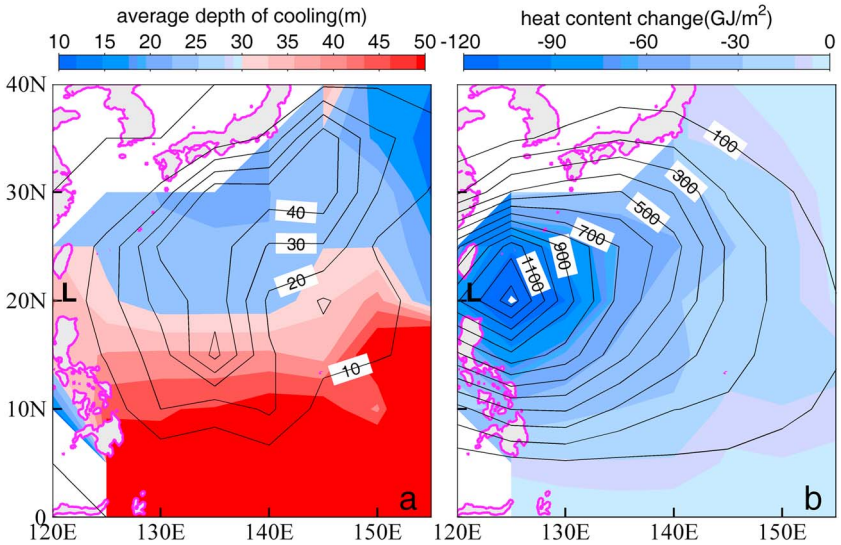

Figure 4. (a) Average depth of TC-induced upper ocean cooling (m, color shading) and distribution of Argo pairs (contours). (b) Accumulated surface heat content change (GJ/m^2, color shading) and the number of all TC centers for all 6 h intervals from 1996 to 2003 (contours).

The composite three-dimensional structure of the cooling for shallow and deep MLDs is illustrated in Figures 3e and 3f, respectively. In shallow MLD regions, the maximum surface cooling is −1.66°C and the cooling depth is 25 m. As expected, the surface cooling is weaker and the maximum cooling depth is deeper in the deep MLD region. The corresponding values are −0.7°C and 40 m, respectively. Morever, the recovery time of the cooling is slightly longer in the shallow MLD than in the deep MLD region because of larger cooling in the shallow MLD region [*Dare and Mcbride*, 2011].

To obtain a complete picture of the cooling induced by northwest Pacific TCs, Figure 4a illustrates the average cooling depth induced by all the TCs during 1996 to 2012. On average, the cooling is deeper south of 25°N than north of 25°N, which is consistent with the spatial pattern of MLD in Figure 1a. This pattern of cooling depth may be caused, in part, by the relatively deeper mixed layer south of 25°N as TC-induced cooling can penetrate to a depth slightly larger than the prestorm MLD [*Large et al*., 1986]. This pattern may also owe, in part, to the finding that TCs south of 25°N are generally stronger (mean V_{max} is 78.7 knots) and slower (mean U_h is 5.74 m/s) than north of 25°N (68.5 knots and 10.5 m/s) (figures are omitted). The accumulated TC-induced heat content change is shown in Figure 4b. Evidently, the heat content change is largest east of Luzon Strait because of the much more active TC occurrences in this region.

4. Conclusions

In this study we analyze Argo profiles of ocean temperature to describe the three-dimensional structure of TC-induced upper ocean cooling in the northwest Pacific. On average, the maximum SST change is approximately −1.4°C, and cooling in excess of 0.5°C can reach ~30 m depth and persist for ~20 days. The cooling can persist longer in the layer between 10 m and 15 m than the other layers.

The magnitude and duration of TC-induced cooling, however, depend on several factors, including TC intensity, translation speed, and MLD. We show that higher intensity and/or slower TCs over the northwest Pacific induce stronger, deeper, and more persistent cooling than lower intensity and/or faster TCs. In the domain of shallow MLD, the surface cooling is generally stronger and the maximum mixing depth is shallower than in the regions of deep MLD. The average cooling depth induced by TCs in the northern part of the domain is shallower than in the southern part. We also have calculated the cooling in different basins such as the North Atlantic. The cooling structure is almost the same, indicating that our finding is robust and can be applicable for all TCs. The findings in this study are useful to understand the response of upper layer ocean to TCs. On longer time scales, our results may be useful to study the role of TCs in the ocean circulation and climate.

This study also demonstrates that Argo is a useful observational network for studying the ocean response to TCs. To gain a better understanding of the high-frequency response to TCs, it would be beneficial to have a sampling interval that is more frequent than currently available with Argo. This suggests that it may be worthwhile to consider high-frequency sampling of the Argo observational network for the study of TCs.

Acknowledgments

The work was supported by the National Basic Research Program of China (2013CB430301), the National Natural Science Foundation of China (41125019, 91428206, and 41306024), and the National Programme on Global Change and Air-Sea Interaction (GASI-IPOVAI-04). N.C.J. was supported by NOAA's Climate Program Office. The Argo data set is from the China Argo Real-time Data Center (http://www.argo.org.cn/), and the data set can be sourced from the international Argo program (http://argo.jcommops.org). TC data set is from the Japanese Meteorological Agency [http://www.jma.go.jp/jma/jma-eng/jma-center/rsmc-hp-pub-eg/trackarchives.html]. Satellite-derived sea surface temperature (SST) data are from the National Oceanic and Atmospheric Administration/National Climate Data Center (ftp://eclipse.ncdc.noaa.gov/pub/OI-daily-v2/NetCDF/). We thank Jim Price at WHOI and the other anonymous reviewer for their constructive comments.

References

ARGO (2000), Argo floats data and metadata from Global Data Assembly Centre (Argo GDAC). Ifremer, doi:10.12770/1282383d-9b35-4eaa-a9d6-4b0c24c0cfc9.

Barcikowska, M., F. Feser, and H. Von Storch (2012), Usability of best track data in climate statistics in the western North Pacific, *Mon. Weather Rev.*, *140*(9), 2818–2830.

Bender, M. A., I. Ginis, and Y. Kurihara (1993), Numerical simulations of the tropical cyclone-ocean interaction with a high-resolution coupled model, *J. Geophys. Res.*, *98*, 23,245–23,263, doi:10.1029/93JD02370.

Black, W. J., and T. D. Dickey (2008), Observations and analyses of upper ocean responses to tropical storms and hurricanes in the vicinity of Bermuda, *J. Geophys. Res.*, *113*, C08009, doi:10.1029/2007JC004358.

Brand, S. (1971), The effects on a tropical cyclone of cooler surface waters due to upwelling and mixing produced by a prior tropical cyclone, *J. Appl. Meteorol.*, *10*, 865–874.

Cione, J. J., and E. W. Uhlhorn (2003), Sea surface temperature variability in hurricanes: Implications with respect to intensity change, *Mon. Weather Rev.*, *131*, 1783–1796.

Dare, R. A., and J. L. Mcbride (2011), Sea surface temperature response to tropical cyclones, *Mon. Weather Rev.*, *139*, doi:10.1175/MWR-D-10-05019.1.

Dickey, T., D. Frye, J. McNeil, D. Manov, N. Nelson, D. Sigurdson, H. Jannasch, D. Siegel, T. Michaels, and R. Johnson (1998), Upper-ocean temperature response to Hurricane Felix as measured by the Bermuda tested mooring, *Mon. Weather Rev.*, *126*, 1195–1201.

Emanuel, K. (2001), Contribution of tropical cyclones to meridional heat transport by the oceans, *J. Geophys. Res.*, *106*, 14, 771–14, 781, doi:10.1029/2000JD900641.

Fisher, E. L. (1958), Hurricanes and the sea-surface temperature field, *J. Meteor.*, *15*, 328–333.

Ginis, I. (2002), Hurricane-ocean interactions, tropical cyclone-ocean interactions, Chapter 3, in *Atmosphere-Ocean Interactions*, *Advances in Fluid Mechanics Series*, vol. 33, edited by W. Perrie, pp. 83–114, WIT Press, Southampton, U. K.

Hart, R. E., R. N. Maue, and M. C. Watson (2007), Estimating local memory of tropical cyclones through MPI anomaly evolution, *Mon. Weather Rev.*, *135*, 3990–4005, doi:10.1175/2007MWR2038.1.
Hazelworth, J. B. (1968), Water temperature variations resulting from hurricanes, *J. Geophys. Res.*, *73*, 5105–5123, doi:10.1029/JB073i016p05105.
Jansen, M. F., R. Ferrari, and T. A. Mooring (2010), Seasonal versus permanent thermocline warming by tropical cyclones, *Geophys. Res. Lett.*, *37*, L03602, doi:10.1029/2009GL041808.
Korty, R. L., K. A. Emanuel, and J. R. Scott (2008), Tropical cyclone-induced upper-ocean mixing and climate: Application to equable climates, *J. Clim.*, *21*, 638–654.
Large, W. G., J. C. Mcwilliams, and P. P. Niiler (1986), Upper ocean thermal response to strong autumnal forcing of the Northeast Pacific, *J. Phys. Oceanogr.*, *16*, 1524–1550.
Leipper, D. F. (1967), Observed ocean conditions and Hurricane Hilda, *J. Atmos. Sci.*, *24*, 182–196.
Lin, I.-I., W. T. Liu, C.-C. Wu, J. C. H. Chiang, and C.-C. Sui (2003), Satellite observations of modulation of surface winds by typhoon-induced upper ocean cooling, *Geophys. Res. Lett.*, *30*(3), 1131, doi:10.1029/2002GL015674.
Lin, I.-I., P. Black, J. F. Price, C.-Y. Yang, S. S. Chen, C.-C. Lien, P. Harr, N.-H. Chi, C.-C. Wu, and E. A. D'Asaro (2013), An ocean coupling potential intensity index for tropical cyclones, *Geophys. Res. Lett.*, *40*, 1878–1882, doi:10.1002/grl.50091.
Mei, W., F. Primeau, J. C. McWilliams, and C. Pasquero (2013), Sea surface height evidence for long-term warming effects of tropical cyclones on the ocean, *Proc. Nat. Acad. Sci.*, *110*, 15,207–15,210.
Nelson, N. B. (1996), The wake of Hurricane Felix, *Int. J. Remote Sens.*, *17*, 2893–2895.
Oey, L.-Y., T. Ezer, D.-P. Wang, S.-J. Fan, and X.-Q. Yin (2006), Loop current warming by Hurricane Wilma, *Geophys. Res. Lett.*, *33*, L08613, doi:10.1029/2006GL025873.
Park, J. J., Y.-O. Kwon, and J. F. Price (2011), Argo array observation of ocean heat content changes induced by tropical cyclones in the North Pacific, *J. Geophys. Res.*, *116*, C12025, doi:10.1029/2011JC007165.
Price, J. F. (1981), Upper ocean response to a hurricane, *J. Phys. Oceanogr.*, *11*, 153–175.
Price, J. F., T. B. Sanford, and G. Z. Forristall (1994), Forced stage response to a moving hurricane, *J. Phys. Oceanogr.*, *24*, 233–260.
Price, J. F., J. Morzel, and P. P. Niiler (2008), Warming of SST in the cool wake of a moving hurricane, *J. Geophys. Res.*, *113*, C07010, doi:10.1029/2007JC004393.
Reynolds, R. W., T. M. Smith, C. Liu, D. B. Chelton, K. S. Casey, and M. G. Schlax (2007), Daily high-resolution-blended analyses for sea surface temperature, *J. Clim.*, *20*(22), 5473–5496.
Roemmich, D., and W. B. Owens (2000), The Argo Project: Global ocean observations for understanding and prediction of climate variability, *Oceanography*, *13*(2), 45–50.
Shay, L. K., P. G. Black, A. J. Mariano, J. D. Hawkins, and R. L. Elsberry (1992), Upper ocean response to Hurricane Gilbert, *J. Geophys. Res.*, *97*, 20, 227–20, 248, doi:10.1029/92JC01586.
Taira, K., S. Kitagawa, H. Otobe, and T. Asai (1993), Observation of temperature and velocity from a surface buoy moored in the Shikoku Basin (OMLET-88)—An oceanic response to a typhoon, *J. Oceanogr.*, *49*, 397–406.
Tong, M. R., Z. H. Liu, C. H. Sun, B. K. Zhu, and J. P. Xu (2003), Analysis of data quality control process of the ARGO profiling buoy, *Ocean Tech.* *22*(4), 79–84. (in Chinese)
Vincent, E. M., M. Lengaigne, J. Vialard, G. Madec, N. C. Jourdain, and S. Masson (2012), Assessing the oceanic control on the amplitude of sea surface cooling induced by tropical cyclones, *J. Geophys. Res.*, *117*, C05023, doi:10.1029/2011JC007705.
Wada, A. (2005), Numerical simulations of sea surface cooling by a mixed layer model during the passage of Typhoon Rex, *J. Oceanogr.*, *61*, 41–57.
Wada, A., J. C. L. Chan (2008), Relationship between typhoon activity and upper ocean heat content, *Geophys. Res. Lett.*, *35*, L17603, doi:10.1029/2008GL035129.
Wada, A., H. Niino, and H. Nakano (2009), Roles of vertical turbulent mixing in the ocean response to Typhoon Rex (1998), *J. Oceanogr.*, *65*, 373–396.
Wang, H. Z., G. H. Wang, D. Chen, and R. Zhang (2012), Reconstruction of three-dimensional Pacific temperature with Argo and satellite observations, *Atmos. Ocean*, *50*(sup1), 116–128.